Challenging the electrostatic σ-hole picture of halogen bonding using minimal models and the interacting quantum atoms approach

Fernando Jiménez-Grávalos[a], Miguel Gallegos[a], Ángel Martín Pendás[a,*], Alexander S. Novikov[b,**]

[a]*Departament of Analytical and Physical Chemistry, University of Oviedo, E-33006, Oviedo, Spain.*
[b]*Saint Petersburg State University, Universitetskaya Nab. 7/9, 199034 Saint Petersburg, Russian Federation*

Abstract

Among the different non-covalent interactions, halogen bonds have captured wide attention in the last years. Their stability has been rationalised in electrostatic terms by appealing to the σ-hole concept, a charge-depleted region that is able to interact favourably with electron rich moieties. This interpretation has been questioned, and in this work a set of anionic halogen model systems are used to shed some light on this issue. We use the Interacting Quantum Atoms (IQA) method, which provides an orbital invariant energy decomposition in which pure electrostatic terms are well isolated, and we complement our insights with the analysis of electrostatic potentials as well as with traditional descriptors of charge accumulation like the Laplacian of the electron density. The total electrostatic interaction between the interacting species is surprisingly destabilising in many of the systems examined, demonstrating that although σ-holes might be qualitatively helpful, much care has to be taken in ascribing the stability of these systems to electrostatics. It is clearly shown that electron delocalisation is essential to understand the stability of the complexes. The evolution of atomic charges as the aggregates form reveals a charge transfer picture in which the central, σ-hole bearing halogen acts as a mere spectator. These systems may then be not far from engaging in a classical 3c-4e interaction. Since the presence of a σ-hole as characterised by the electrostatic potential mapped on a suitable molecular envelope isosurface does not guarantee attractive electrostatic interactions, we encourage to employ a wider perspective that takes into account the full charge distribution.

---

*To whom correspondence should be addressed: ampendas@uniovi.es
**To whom correspondence should be addressed: a.s.novikov@spbu.ru

1. Introduction

The consideration of non-covalent interactions (NCIs) is one of the priority development directions in modern chemistry and related areas of natural science. The attention of the scientific community to this field has grown explosively in the past decade, as these weak contacts play key roles in most chemical[1–3] and biochemical[4,5] processes. Non-covalent interactions determine the existence of molecular solids and the properties of molecular systems in the gas and liquid phases, and their control has found wide application in nanoscience,[6,7] material science,[8,9] medicine[10,11] or catalysis,[12–16] to name just a few fields. As progress accumulates, the number of purportedly new NCIs beyond the ubiquitous van der Waals attractions has increased considerably, and the NCI zoo now includes beryllium, tetrel, pnictogen, chalcogen, etc. bonds.[17–20] In many of these, electrostatic interactions have been targeted as fundamental, and the concept of σ-holes has become instrumental,[21–23] particularly in halogen bonds.[24,25]

It has thus become generally accepted that the charge density anisotropy of bonded halogen atoms leading to σ-holes is the driving force behind halogen bonding. This has lead to emphasise the role of the molecular electrostatic potential (ESP) in understanding these interactions,[26] and to assume that their energetics should be well described by classical contributions.[27] Nonetheless, such a traditional view has been challenged in the last few years with the use of other complementary techniques.

In this respect, numerous computational studies have appeared trying to shed light on the nature of halogen-bond (XB) interactions. Most are based on orbital-based energetic decompositions that use natural bond orbitals (NBO), Kohn-Sham based energy decomposition analyses (EDA), block-localised wave functions (BLWs), in the realm of valence bond (VB) theory, or even symmetry adapted perturbation theory (SAPT).[22,25,28–33] Less effort has been put in rationalising halogen bonding with orbital invariant real space-based alternatives, such as the interacting quantum atoms (IQA) scheme.[34,35] Fock-space analyses already warned about the importance of non-purely electrostatic contributions, such as charge transfer, polarisation, or dispersion in different complexes.[22,25,28–33] On the other hand, the IQA picture has also revealed how in some instances covalent effects, as revealed by non-negligible exchange-correlation energies, may have been skipped.[32,36–44]

In this work, we have decided to adhere to Occam's razor arguments [Johannes Poncius' commentary on John Duns Scotus' Opus Oxoniense, book III, dist. 34, q. 1. in John Duns

Scotus Opera Omnia, vol. 15, Ed. Luke Wadding, Louvain (1639), reprinted Paris: Vives, (1894) p.483a] and thus to choose the simplest possible model systems of halogen bonding in order to isolate as well as possible the driving forces behind their stability through the IQA partitioning. Since XBs comprise a σ-hole bearing halogen atom acting as a Lewis acid that interacts with a Lewis base counterpart, we opted to explore the σ-hole halogen interactions within negatively charged $X_1 - Y_2 - X_3$ species, using different combinations of chlorine, bromine and iodine as the X and Y moieties.

According to the early work of Sakurai[45] and Desijaru,[46] and the seminal paper by Espinosa and coworkers on halogen-halogen interactions,[47] there would be two distinct geometrical arrangements for two interacting halogens in crystals. The first one, called type I, refers to a symmetric, often linear arrangement that occurs mainly around a crystallographic inversion centre and is generally regarded to be dispersion driven. In the second, or type II, the interaction occurs at angles close to 90°, and the positively-charged σ-hole from one atom approaches the negative lone pair belt of the other, so that electrostatic terms are expected to dominate. Type II XBs are often found on crystallographic screw axes and glide planes. In order to capture the mutual effect of maximised van der Waals forces in type I and electrostatic interactions in type II geometries, we selected linear geometries between a halogen diatomic molecule and an approaching halide ion.

To decrease the number of degrees of freedom as much as possible, we have inspected both the potential energy surface minima, corresponding to the symmetric $[X_1 - Y_2 - X_3]^-$ trihalide configurations as found in the gas phase (Figure 1b), and constrained $X_1 - Y_2 \cdots X_3^-$ asymmetric geometries that mimic the halogen arrangements found in crystals (Figure 1a). These systems are close to those studied by Wolters and Bickelhaupt with Kohn-Sham EDAs,[48] that were also chosen thanks to their capturing of the essence of σ-holes and XBs.

Thus, and with all the previous simplifications, we seek to compare the role of σ-holes in XBs from different perspectives: the qualitative picture provided by the ESP and other scalar fields like the Laplacian of the electron density, and the quantitative image given by the IQA energetic decomposition. IQA has now been used to shed light on a wide variety of phenomena, including some recent controversies such the nature of bonding in anion-π interactions or the character of the Na-B bond in $NaBH_3^-$ to cite a couple of them.[49,50] This together with its orbital-invariant nature makes it an appropriate choice for our study. In doing so, we expect to gain deeper insight into the nature of halogen bonding as well as to check whether the electrostatic view

survives quantitative analyses.

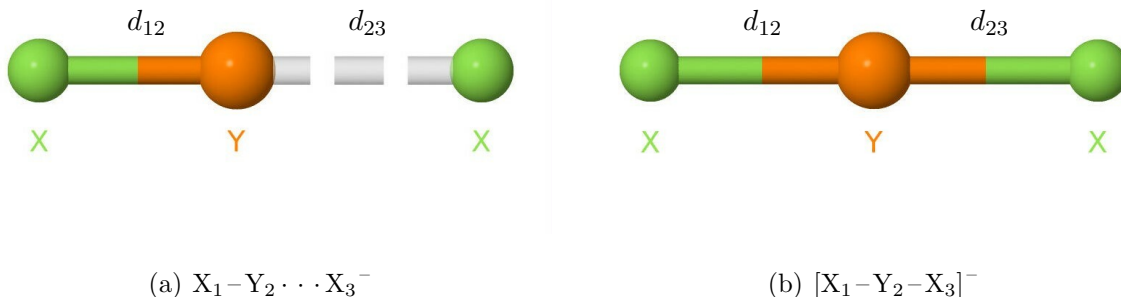(a) $X_1-Y_2\cdots X_3{}^-$ (b) $[X_1-Y_2-X_3]^-$

Figure 1: Geometries considered in this work: constrained asymmetric complex (left), with $d_{12} < d_{23}$, and symmetric trihalide (right) structure, with $d_{12} = d_{23}$.

2. Methodology

Quantum Chemical Topology (QCT) refers to a set of wave function analysis techniques that take advantage of the topology induced by the gradient field of orbital invariant descriptors.[51] By construction, QCT is independent on the electronic structure method selected to build the system's wave function. Amongst the most well-known QCT procedures we find the Quantum Theory of Atoms in Molecules (QTAIM) of Bader et al.,[52] which provides an atomic-like exhaustive partition of real space and of the expectation values of any quantum mechanical operator. In the QTAIM, atoms are defined as the attractor basins of the electron density field, $\rho(\boldsymbol{r})$. A general energy partition scheme in QCT that leads to an atomic and interatomic decomposition of the molecular energy when applied to the QTAIM is the interacting quantum atoms (IQA) approach.[34,35] IQA/QTAIM provides physically rigorous domain kinetic energies, in contrast to those offered by other spatial decompositions, and it needs only the first- and second-order reduced density matrices to compute its different energy terms. According to this scheme, and making use of its usual language, the total energy E is split into a sum of atomic (net) energies E_{net}^A and pairwise additive interaction terms E_{int}^{AB} as

$$E = \sum_A E_{net}^A + \sum_{A<B} E_{int}^{AB}. \tag{1}$$

The atomic net-energy comprises, on the one hand, the kinetic energy of the electrons contained in a particular basin, their mutual interaction, and the attraction with the particular

nucleus they are associated with. On the contrary, E_{int}^{AB} gathers the interactions of all the electrons and nuclei located in a basin A with those located in basin B.

There are two sources for the interaction energy, namely the classical electrostatic interaction between the total (nuclear and electronic) charge densities lying in the A and B regions, and a correction to that term which is purely quantum mechanical in nature. Accordingly, the interaction energy can be separated into a Coulomb, or classical contribution E_{cl}^{AB} —that has been shown to correspond to the ionic component of a chemical interaction— and an exchange-correlation one E_{xc}^{AB} —that measures covalency:

$$E_{int}^{AB} = E_{cl}^{AB} + E_{xc}^{AB}. \tag{2}$$

Related with the exchange-correlation energy is the delocalisation index, DI. It corresponds to the integration of the exchange-correlation density over two basins and is the real space equivalent of bond order, whose value can be interpreted as the number of electron pairs that two particular basins share.[53]

Since the union of QTAIM regions is again a proper QTAIM domain, we can gather sets of QTAIM atoms to form groups $\mathcal{G}$ and rewrite the IQA partitioning in terms of them:

$$E = \sum_{\mathcal{G}} E_{net}^{\mathcal{G}} + \sum_{\mathcal{G} < \mathcal{H}} E_{int}^{\mathcal{G}\mathcal{H}}, \tag{3}$$

with

$$E_{net}^{\mathcal{G}} = \sum_{A \in \mathcal{G}} E_{net}^{A} + \sum_{\substack{A < B \\ A,B \in \mathcal{G}}} E_{int}^{AB} \tag{4}$$

$$E_{int}^{\mathcal{G}\mathcal{H}} = \sum_{\substack{A < B \\ A \in \mathcal{G}, B \in \mathcal{H}}} E_{int}^{AB}. \tag{5}$$

Here, $\mathcal{G}$ and $\mathcal{H}$ stand for the different groups in which the molecule has been divided. The same grouping can be performed for each of the different IQA energy components, such as the classical or exchange-correlation contributions.

The unavailability of a second-order reduced density matrix in DFT prevents the exact decomposition of the exchange-correlation energy in an IQA-like manner, hence DFT would not be in principle compatible with IQA. Nevertheless, several working approximations have been introduce to by-pass this limitation. Here we will consider a scaling technique that modifies both intra- and interatomic contributions.[54]

Given a particular exchange-correlation functional with a non-hybrid part $\epsilon(\mathbf{r})$, the total DFT exchange-correlation (xc) energy can be easily computed as

$$E_{xc}^{DFT} = \int_{\mathbb{R}^3} \rho(\mathbf{r})\epsilon(\mathbf{r})d\mathbf{r} + a_0 E_x^{KS}, \tag{6}$$

where a_0 denotes the fraction of the pure Hartree-Fock (HF) exchange E_x^{KS}, which is directly computed from the Kohn-Sham (KS) orbitals when a hybrid functional is used.

By delimiting the previous integral to a particular spacial basin (e.g., Bader's atomic regions, with $\mathbb{R}^3 = \cup_A \Omega_A$), a splitting of the total xc energy is achieved, but such terms involve both IQA intra- and inter-basin contributions. To overcome this problem a scaling technique based on the E_{xc}^{DFT}/E_x^{KS} ratio over each basin was successfully proposed.[54] First, the parameters λ_A must be computed for each atomic basin as

$$\lambda_A = \frac{E_{xc,add}^{DFT,A}}{E_{x,add}^{KS,A}} = a_0 + \frac{1}{E_{x,add}^{KS,A}} \int_{\Omega_A} \rho(\mathbf{r})\epsilon(\mathbf{r})d\mathbf{r}, \tag{7}$$

where add stands for the additivity of the terms, as they sum up to the molecular E_{xc}^{DFT} and involve inter- and intra-atomic components. The Hartree-Fock exchange is calculated with the sum

$$E_{x,add}^{KS,A} = E_x^{KS,A} + \frac{1}{2}\sum_{B\neq A} E_x^{KS,AB}, \tag{8}$$

where

$$E_x^{KS,AB} = \int_{\Omega_A} d\mathbf{r}_1 \int_{\Omega_B} d\mathbf{r}_2 r_{12}^{-1} \rho_x^{KS}(\mathbf{r}_1, \mathbf{r}_2), \tag{9}$$

that corresponds to the intra-atomic $E_x^{KS,A}$ for $\Omega_B \equiv \Omega_A$ and only requires the set of KS molecular orbitals to construct the exchange density $\rho_x^{KS}(\mathbf{r}_1, \mathbf{r}_2)$.

Once the set of λ_A parameters is available, these are utilised to approximate the intra- ($B = A$) or inter-atomic ($B \neq A$) DFT xc energies as follows:

$$\tilde{E}_{xc}^{AB} = \frac{1}{2}\left[\lambda_A + \lambda_B\right] E_{x,add}^{KS,A}. \tag{10}$$

Consequently, the xc energy is split into

$$E_{xc}^{DFT} = \sum_A \tilde{E}_{xc}^A + \sum_{B\neq A} \tilde{E}_{xc}^{AB}. \tag{11}$$

Traditionally, σ-hole driven halogen bonding has been characterised in terms of the positive ESP region that develops along the bonding axis in heavy halogens that usually points toward the lone pair torus of their bonding partners.[55,56] Any real space measure of electron localisation

like the electron localisation function (ELF),[57] or of local charge concentration and depletion, like the Laplacian of the electron density $\nabla^2\rho$, can be used to explore and detect σ-holes trustfully.[58–60] As the Laplacian is regarded, its ability to uncover the shell structure of low Z atoms makes it a very appealing descriptor. Even for ($Z \geq 20$) atoms, for which the Laplacian does not resolve their valence shells appropriately, the visualisation of $\nabla^2\rho$ still provides clear pictures of σ-hole behaviour.

3. Computational details

Geometry optimisations and single point calculations were carried out with the Gaussian09 (G09) package[61] at the M06-2X/x2c-TZVPPall level of theory, with Grimme's D3 dispersion correction[62] and an ultrafine grid. The M06-2X density functional was specifically developed and parameterised for a correct description of non-covalent interactions (especially in the case of main group chemical elements)[63] and was also validated for these purposes in several benchmark studies.[64–66] We have chosen this functional according to our previous experience and its successful performance in a number of halogen bond studies in various similar supramolecular systems.[67–71]

In order to avoid problems with relativistic effects, we used the specially developed segmented contracted all-electron relativistic basis sets x2c-TZVPPall and the Ahlrich's family basis sets def2-TZVPP with all-electron spin-free X2C correction for iodine.[72] We have also previous experience on the successful application of such basis sets in studies of non-covalent interactions[73,74] and, in particular, in chemical systems containing heavy atoms (noble metals, iodine).[75,76] Additionally, the RESC scalar relativistic approach,[77] as implemented in G09, was employed for all compounds that include iodine.

All the optimisations converged towards the trihalides $[X_1-Y_2-X_3]^-$, that were properly characterised through harmonic frequency analysis. To obtain asymmetric geometries $X_1-Y_2\cdots X_3{}^-$ resembling the arrangements found in crystals, a scan over the Y_2-X_3 distance was performed with a frozen X_1-Y_2 separation equal to the experimental diatomic equilibrium one, retrieved from the NIST database.[78] This has proven to be a reliably procedure to examine pure halogen bonding effects without the influence of further species.

Analogously, and in order to test the reliability of the DFT results, a comparison between the energy components of M06-2X and a more reliable CCSD reference was also performed. For these correlation-consistent calculations, PySCF[79] was used to obtain the density matrices

required by the subsequent IQA analyses. The x2c-TZVPPall and def2-TZVPP were used in these calculations for a selected set of $X_1-Y_2 \cdots X_3^-$ systems. Also, relativistic effects were accounted for iodine compounds, in this case with the all-electron spin-free X2C correction. This precludes a complete IQA reconstruction of the energy, but does not affect the interatomic interaction components, which constitute our focus.

The wave functions obtained from the previous G09 or PySCF calculations were input to the `PROMOLDEN` code[80] to carry out the IQA energetic analyses. For these, β-spheres with radii between 0.30 and 0.35 a.u. were employed along with 5810-point Lebedev angular grids and Gauss-Chebychev of 2nd kind radial quadratures with 451 radial points. The expansion of r_{12}^{-1} was performed up to a L_{max} of 10. Non β-sphere grids were performed using the same angular quadratures but 551 points Clenshaw-Curtis radial quadrature was chosen in this case and the L_{max} was raised to 12. `PROMOLDEN` does not actually recover relativistic effects, that would affect mainly some intra-basin energy contributions like the atomic kinetic energy. Since we are mainly interested in interatomic interaction energies, which remain basically unperturbed after our relativistic calculations, we think that the reported interactions involving iodine atoms are not seriously affected by this approximation.

Finally, the molecular and atomic representations have been obtained with the AIMAll[81] and Jmol[82] codes. The rest of the figures were done with the help of Python's Matplotlib.[83]

4. Results and Discussion

4.1. Systems

As mentioned in the Introduction, we have focused our efforts on pure negatively-charged halogen species that are intended to capture the essence of σ-hole interactions. These systems bind linearly through the extra σ-like lone pair of the halide anion. A total of eighteen of these systems have been considered in this work. These comprise the trihalides as well as the constrained X_1-Y_2 dimers attacked by a X_3 halogen anion in a linear arrangement,[47] where X,Y=Cl, Br, I: $Cl-Cl\cdots Cl^-$, $[Cl-Cl-Cl]^-$, $Cl-Br\cdots Cl^-$, $[Cl-Br-Cl]^-$, $Cl-I\cdots Cl^-$, $[Cl-I-Cl]^-$, $Br-Br\cdots Br^-$, $[Br-Br-Br]^-$, $Br-Cl\cdots Br^-$, $[Br-Cl-Br]^-$, $Br-I\cdots Br^-$, $[Br-I-Br]^-$, $I-Cl\cdots I^-$, $[I-Cl-I]^-$, $I-Br\cdots I^-$, $[I-Br-I]^-$, $I-I\cdots I^-$, $[I-I-I]^-$. We leave aside fluorine, since this element is normally not considered to get involved in halogen bonds as a result from its low polarisability. All optimised and constrained geometries and energies can be found in the Supporting Information (SI), Table S1.

8

4.2. Atomic charges and interatomic interaction energies

Sigma holes are expected to enhance halogen interactions by means of favourable electrostatics between the halogen that develops the σ-hole and the attacking, electron-rich moiety. However useful any argument based on the docking of ESP isosurfaces may be, it is always the total electrostatic interaction between the approaching entities that has to be taken into account. This is something that IQA provides directly. As we are going to show, a lock-and-key ESP isosurface match may actually hide a globally destabilising electrostatic contribution. The IQA interaction energy E_{int}^{AB}, and its classical (Coulomb, E_{class}) and non-classical (exchange-correlation, E_{xc}) components give directly the grand total interactions, which can be perceived as what one would obtain if we brought together all the ESP pictures at all possible different isovalues, reconstructing an onion from its peels. Another way to state this idea comes from recognising that a region characterised by a positive ESP value on the van der Waals envelope surface may well display a negative ESP value on another surface, so that the global electrostatic is by no means obvious from the exam of the first surface.

Table 1 contains the total interaction energies, along with the classical and exchange-correlation contributions, for every pair of atoms present in the complexes. The QTAIM atomic charges are also depicted. Although the data present in Table 1 correspond to the M06-2X density functional, we have validated the reliability of our results by performing reference CCSD calculations on a selected number of systems: $Cl-Cl\cdots Cl^-$, $Cl-Br\cdots Cl^-$, $Cl-I\cdots Cl^-$ and $Br-Br\cdots Br^-$, with both the x2c-TZVPPall and the def2-TZVPP basis sets. The data can be found in the S2 and S3 Tables of the SI. Small differences in charges and larger energetic discrepancies can be found on comparing the DFT and CCSD data but, overall, the M06-2X/x2c-TZVPPall level of theory so far used is found to be accurate enough. All trends found in Table 1 are maintained. For comparison purposes also, M06-2X results in the optimised *in vacuo* X_1-Y_2 diatomics can also be found in Table 2.

Table 1: Atomic charges (a.u.) as well as delocalisation indices (DI) and interaction energies (in kcal mol^{-1}) for each atomic pair in the complexes $X_1-Y_2-X_3$ at the M06-2X/x2c-TZVPPall level. Negative charges are coloured in red, positive in blue and those close to zero in green.

Complex	Pair	DI	E_{int}	E_{xc}	E_{class}
$Cl_1^{-0.30}-Cl_2^{+0.04}\cdots Cl_3^{-0.74}$	1-2	1.278	-161.439	-182.490	21.051
	2-3	0.542	-66.779	-60.613	-6.166
	1-3	0.149	6.863	-5.443	12.306
$[Cl_1^{-0.50}-Cl_2^{+0.01}-Cl_3^{-0.50}]$	1-2	0.872	-104.724	-107.164	2.440
	2-3	0.872	-104.502	-107.169	2.667
	1-3	0.211	7.861	-7.646	15.507
$Cl_1^{-0.46}-Br_2^{+0.16}\cdots Cl_3^{-0.70}$	1-2	1.169	-159.842	-156.455	-3.387
	2-3	0.674	-94.116	-76.965	-17.151
	1-3	0.152	15.019	-5.443	20.462
$[Cl_1^{-0.56}-Br_2^{+0.12}-Cl_3^{-0.56}]$	1-2	0.877	-113.753	-104.485	-9.268
	2-3	0.877	-113.916	-104.551	-9.366
	1-3	0.179	13.500	-6.234	19.734
$Cl_1^{-0.61}-I_2^{+0.34}\cdots Cl_3^{-0.73}$	1-2	1.061	-174.495	-130.451	-44.044
	2-3	0.696	-115.651	-75.887	-39.764
	1-3	0.118	25.321	-4.003	29.324
$[Cl_1^{-0.65}-I_2^{+0.30}-Cl_3^{-0.65}]$	1-2	0.836	-128.549	-93.217	-35.332
	2-3	0.835	-128.068	-93.114	-34.955
	1-3	0.129	22.938	-4.229	27.167
$Br_1^{-0.22}-Cl_2^{-0.10}\cdots Br_3^{-0.69}$	1-2	1.243	-142.250	-165.847	23.597
	2-3	0.590	-58.304	-64.176	5.872
	1-3	0.192	-0.491	-6.571	6.080
$[Br_1^{-0.45}-Cl_2^{-0.10}-Br_3^{-0.45}]$	1-2	0.883	-93.221	-103.455	10.234
	2-3	0.881	-93.034	-103.235	10.201
	1-3	0.251	2.311	-8.476	10.787
$Br_1^{-0.39}-Br_2^{+0.03}\cdots Br_3^{-0.64}$	1-2	1.164	-132.598	-147.432	14.835
	2-3	0.729	-83.199	-81.060	-2.139
	1-3	0.191	7.152	-6.407	13.559

$[Br_1^{-0.50}-Br_2^{+0.01}-Br_3^{-0.50}]$	1-2	0.883	-98.024	-102.562	4.538
	2-3	0.881	-98.239	-102.832	4.593
	1-3	0.251	7.136	-7.004	14.141
$Br_1^{-0.52}-I_2^{+0.21}\cdots Br_3^{-0.69}$	1-2	1.099	-139.381	-127.528	-11.854
	2-3	0.698	-92.092	-71.456	-20.636
	1-3	0.147	16.688	-4.536	21.224
$[Br_1^{-0.59}-I_2^{+0.18}-Br_3^{-0.59}]$	1-2	0.857	-104.986	-90.242	-14.744
	2-3	0.857	-105.079	-90.311	-14.768
	1-3	0.161	15.456	-4.857	20.312
$I_1^{-0.06}-Cl_2^{-0.28}\cdots I_3^{-0.66}$	1-2	1.208	-141.696	-147.381	5.685
	2-3	0.542	-37.715	-53.691	15.975
	1-3	0.24	-9.262	-7.409	-1.853
$[I_1^{-0.37}-Cl_2^{-0.26}-I_3^{-0.37}]$	1-2	0.853	-80.019	-92.052	12.033
	2-3	0.851	-79.783	-91.862	12.080
	1-3	0.317	-3.618	-9.734	6.116
$I_1^{-0.24}-Br_2^{-0.15}\cdots I_3^{-0.61}$	1-2	1.168	-117.898	-135.958	18.060
	2-3	0.661	-58.258	-66.461	8.204
	1-3	0.237	-1.622	-7.156	5.533
$[I_1^{-0.42}-Br_2^{-0.16}-I_3^{-0.42}]$	1-2	0.872	-79.271	-91.298	12.027
	2-3	0.873	-79.488	-91.397	11.909
	1-3	0.274	0.301	-8.108	8.409
$I_1^{-0.41}-I_2^{+0.04}\cdots I_3^{-0.63}$	1-2	1.129	-112.387	-123.099	10.712
	2-3	0.719	-73.745	-69.966	-3.779
	1-3	0.192	7.315	-5.485	12.801
$[I_1^{-0.51}-I_2^{+0.02}-I_3^{-0.51}]$	1-2	0.879	-84.009	-87.520	3.512
	2-3	0.879	-84.689	-87.474	2.785
	1-3	0.209	7.356	-5.846	13.202

Table 2: Atomic charges (a.u.), delocalisation indices (DI), exchange-correlation, classical and total interaction energies (kcal mol^{-1}) for the *in vacuo* diatomic molecules X_1-Y_2. Negative charges are coloured in red, positive in blue and those close to zero in green.

Diatomic molecule	DI	E_{int}	E_{xc}	E_{class}
$Cl^{0.00}-Cl^{0.00}$	1.440	-170.066	-199.990	29.923
$Cl^{-0.14}-Br^{+0.14}$	1.407	-164.855	-181.860	17.006
$Cl^{-0.33}-I^{+0.33}$	1.323	-178.780	-155.429	-23.351
$Br^{0.00}-Br^{0.00}$	1.415	-148.233	-172.478	24.245
$Br^{-0.20}-I^{+0.20}$	1.367	-146.100	-151.289	5.188
$I^{0.00}-I^{0.00}$	1.395	-125.317	-144.553	19.236

A most remarkable feature found in both the trihalides and the halogen-bonded moieties is the considerable value of the charge difference in the edge atoms $\Delta Q(\text{X3}) \sim -\Delta Q(\text{X1})$, measured from the isolated $\text{X}_1 - \text{Y}_2$ reference. This can be naïvely interpreted as a direct charge transfer from the attacking halide X_3 to the farthermost halogen atom X_1. In the symmetric trihalide systems, the central Y_2 atom is almost neutral if X=Y, and carries a positive or negative charge, consistent with the difference of electronegativity between X and Y, otherwise. In any case, the anionic character of all the molecules is heavily carried by the external X atoms. Interestingly, this large density polarisations are also found in the asymmetric $\text{X}_1 - \text{Y}_2 \cdots \text{X}_3^-$ systems that we use to model halogen bonds, albeit the attacking X_3^- now retains a larger part of the anionic negative charge. Despite the distance between Y_2 and X_3, that we will call d_{23}, is longer than d_{12} in the $\text{X}_1 - \text{Y}_2 \cdots \text{X}_3^-$ systems mimicking halogen bonding (see Table S1), the central charge is pretty similar for Y_2 in both $[\text{X}_1 - \text{Y}_2 - \text{X}_3]^-$ and $\text{X}_1 - \text{Y}_2 \cdots \text{X}_3^-$. More interestingly, this central charge resembles to a large extent that found in the corresponding isolated diatomic molecule. This shows very neatly that this edge to edge polarisation is rather general and that the central atom plays an spectator role as far as electrostatics is concerned. We will consider more deeply this issue in the next section.

Contrary to the common assumption that the covalent or exchange-correlation contribution is not very relevant in comparison with its electrostatic counterpart in σ-hole interactions, IQA shows that such an energy component is of great importance in all the cases studied. This is in line with previous assessment of the role of both type of interactions in other σ-hole instances.[32,36–44] A close inspection of the pair interaction energies and their components reveals that the 2-3 pairs are many times destabilised by the electrostatic term and that, even when those energies are stabilising, the non-classical ones always dominate. The closer the third X_3 atom is to Y_2, the more attractive the $\text{X}_3 - \text{Y}_2$ interactions become, but at the expense of increasing the repulsive character of the Coulomb interactions while the xc term becomes even more dominant. It shall be seen in following sections that the grouped attractive interaction of fragment 1-2 with atom 3 is explained only by the E_{xc} component in almost all the cases studied, whilst the group E_{class} terms are destabilising.

Paying attention to the relation between the electrostatic interaction and the monopole $Q^A Q^B / R_{AB}$ contribution, our results show that, in general, oppositely charged basins lead to stabilising electrostatics, although multipolar terms often modify this initial assumption. For example, the first two chlorine atoms of $\text{Cl} - \text{Cl} \cdots \text{Cl}^-$ present an E_{class} of $\sim +21$ kcal mol^{-1}

although the involved atoms carry opposite-sign net charges. Multipolar contributions are only dominant when one of the two species displays small net charges.

It is also relevant to consider how the $X_1 - Y_2$ pair becomes modified when passing from the isolated diatomic to the $X_1 - Y_2 \cdots X_3{}^-$ systems, since the distance between the first two atoms remains fixed in this process. It is clear that, in general, $E_{int}(X_1, Y_2)$ becomes less favourable as the X_3 atom approaches. The smallest destabilisations in E_{int} are found for systems with X=Cl and Y=I, ranging from 4.3 ($Cl-I \cdots Cl^-$) to 12.9 kcal mol^{-1} ($I-I \cdots I^-$); the largest ones in the opposite X=I and Y=Cl situations, the I-Cl interaction in $I-Cl \cdots I^-$ being that which is mostly destabilised (by 31.1 kcal mol^{-1}). Concerning its components, $|E_{xc}(X_1 Y_2)|$ decreases upon interaction, an easy to interpret result since the central Y_2 atom now shares its valence electrons among two, and not one species. In most cases, the xc destabilisation is larger than that found in the total E_{int}. On the other hand, $E_{class}(X_1, Y_2)$ shows a richer behaviour. In some cases the electrostatic interaction weakens, but in others it strengthens substantially. This is in accordance with the charge transfer that the diatomic molecule undergoes upon complex formation. For instance, in Cl-Br, $Q(Cl) = -0.14e$. When moving to the complexes, in $Cl-Br \cdots Cl^-$ bromine maintains roughly the same charge, while chlorine gains about 0.46 e and, accordingly, their mutual classical energy stabilises by about 20 kcal mol^{-1}. Contrarily, in $Br-Cl \cdots Br^-$, bromine bears a charge of -0.45 e, but, at the same time, chlorine gains 0.10 extra electrons, giving rise to a electrostatic destabilisation of 6.6 kcal mol^{-1}. Similar trends are found for the rest of the $X_1 - Y_2 \cdots X_3{}^-$ systems.

As d_{23} is considerably smaller in the trihalides, their associated E_{xc} (and so E_{int}) values are rather larger than those present in the asymmetric complexes. The most stabilising E_{class} is found in $Cl-I \cdots Cl^-$, where the more compact and polarisant Cl^- ion interacts with the diffuse, polarisable I atom. The same behaviour is found in Br, although in a less pronounced fashion. Since the interaction of Y with both X is symmetric, and so are distances d_{12} and d_{23}, the $X_1 - Y_2$ bond is highly weakened, with an E_{int} destabilisation ranging from 41.1 to 98.8 kcal mol^{-1}. The major source of destabilisation is again E_{xc}, in accordance with the loss in electron sharing (57.0-92.8 kcal mol^{-1}), while E_{class} turns out again to be the most interesting contribution to the 1-2 pair interaction energy. For all systems but $[I-Cl-I]^-$ and $[I-Br-I]^-$ the electrostatic interaction energy of pairs 1-2 stabilises from 6.7 (in $[Br-Cl-Br]^-$) to 27.5 kcal mol^{-1} (in $[Cl-Cl-Cl]^-$). $[I-Cl-I]^-$ and $[I-Br-I]^-$, by contrast, show an E_{class} destabilisation of 6.8 and 35.4 kcal mol^{-1} respectively. This is as a result of the large multipolar distortions
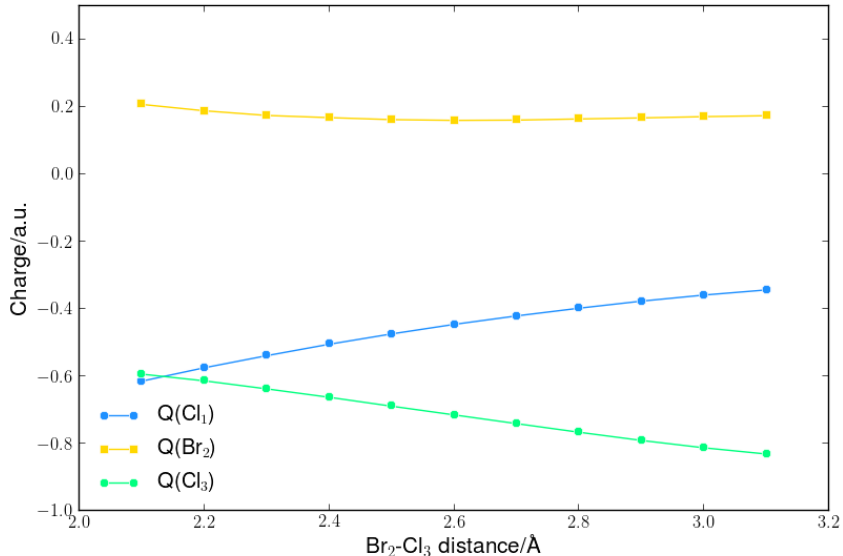
suffered by the iodine atoms.

All the previous findings concerning the charge distribution and the high relative importance of the xc energy in the systems here studied are in line with the Pimentel-Rundle model,[84,85]. In real space, the effects of the 3c-4e bond translates into anomalously high delocalisation indices between the edge atoms,[86] and it also predicts net charges equal to $-0.5\,e$ for the external atoms. All this is in very good agreement with what we have obtained in the $[X_1-Y_2-X_3]^-$ species as shown in Fig. 1. More interestingly, these insights remain valid with slight modifications in the $X_1-Y_2\cdots X_3{}^-$ complexes. The incipient formation of a 3c-4e-like interactions in halogen bonds is thus a possibility that should be further studied with standard orbital techniques. For instance, Oliveira et al. used relative stretching force constants in this regard.[87] The presence of such a bond type justifies the real space image and strengthens the importance of quantum mechanical contributions on top of the dominant electrostatic point of view.

4.3. Charge transfer along $Y_2-X_3{}^-$ stretching

One of the most striking features highlighted in the previous section is the large charge transfer following the approach of the $X_3{}^-$ anion. It leads to the farthermost X_1 atom concentrating the charge excess while the central atom Y_2 maintaining a quite similar charge to that it carries in the isolated diatomic molecule. In order to assess whether this observation is the result of a concerted charge transfer mechanism in which the central atom is not directly affected, or one with several steps in which CT and polarisation are decoupled, several scans over the Y_2-X_3 distance were performed for the systems $Cl-Cl\cdots Cl^-$, $Cl-Br\cdots Cl^-$, $Cl-I\cdots Cl^-$ and $Br-Br\cdots Br^-$. Figure 2 depicts the evolution of the atomic charge for each atom in the $Cl-Br\cdots Cl^-$ complex (the rest of the selected systems and the CCSD reference calculations can be found in Table S4).

In the distance range sampled, it is rather clear that the charge of the central atom does not change appreciably while, on the contrary, the external atoms display mirror evolutions. Similar results are found for the rest of the systems considered. This experiment demonstrates that the $X_3{}^-$ to X_1-Y_2 charge transfer is in this region a one-step process, which cannot be easily explained without the assistance of orbital interactions. Whether this is a particular feature of halide attacks or a general property of halogen bonds remains a very important point to be investigated. If these results are found to be general, the full halogen bonding electrostatic model will have to be reconsidered. It is interesting to note that the evolution of $Q(X_3)$ with

15

Figure 2: Atomic charges (in a.u.) as a function of the $Br \cdots Cl$ distance.

distance is convex in the case of Y=Cl but that it changes to concave when more bulky atoms become involved. Thus, for Y=Br the trend is quasi-linear (such as the case depicted in Fig. 2), and clearly concave between external Cl and central I (also more charged terminal Cl). Such a behaviour reveals the rate at which the charge transfer takes place, that results more rapid when more accessible (i.e., compact) atoms occupy the central position.

4.4. IQA formation energies

The formation energies (E_{form}) that provide the stabilisation energy of the trihalide or asymmetric complexes from the isolated diatomics and halide ions can also be partitioned within the IQA approach. E_{form} thus becomes a sum of the deformation energy of the fragments E_{def} —the energetic cost needed to prepare the fragment from its *in vacuum* energy to the geometric and electronic state found within the complex— and the interaction energy between the two fragments. Additionally, an IQA equivalent of Pauli repulsion in weakly interacting systems can be built by adding the fragments total deformation to their mutual exchange-correlation energy. This is usually known as the exchange-correlation repulsion term, XCR $= E_{def}(X_1 - Y_2) + E_{def}(X_3) + E_{xc}(X_1 - Y_2, X_3)$. This IQA fragment partition can be found in Table 3.

The set of formation energies provided by IQA (E_{form}^{IQA}) are very close to the ones calculated from the G09 package (E_{form} in Table S1), although subject to a certain numerical error. Notice

16

Table 3: IQA formation energies obtained from the balance between the deformation of fragments X_1-Y_2 and X_3, and their mutual interaction, together with their exchange-correlation repulsion terms XCR. All data in kcal mol^{-1}.

Complex	E_{form}^{IQA}	$E_{def}(X_1-Y_2/X_3)$	E_{int}	E_{xc}	E_{class}	XCR
$\mathbf{Cl-Cl\cdots Cl^-}$	-21.608	14.178 / 24.131	-59.917	-66.057	6.140	-27.748
$\mathbf{[Cl-Cl-Cl]^-}$	-28.764	14.287 / 53.591	-96.641	-114.815	18.174	-46.937
$\mathbf{Cl-Br\cdots Cl^-}$	-32.643	14.100 / 32.354	-79.097	-82.408	3.311	-35.954
$\mathbf{[Cl-Br-Cl]^-}$	-39.277	11.384 / 49.755	-100.416	-110.785	10.369	-49.646
$\mathbf{Cl-I\cdots Cl^-}$	-35.470	21.592 / 33.268	-90.330	-79.889	-10.440	-25.030
$\mathbf{[Cl-I-Cl]^-}$	-40.276	21.018 / 43.837	-105.130	-97.342	-7.788	-32.488
$\mathbf{Br-Cl\cdots Br^-}$	-22.142	10.669 / 25.985	-58.795	-70.747	11.952	-34.094
$\mathbf{[Br-Cl-Br]^-}$	-29.010	6.754 / 54.959	-90.723	-111.711	20.988	-46.998
$\mathbf{Br-Br\cdots Br^-}$	-32.530	9.778 / 33.739	-76.047	-87.467	11.421	-43.951
$\mathbf{[Br-Br-Br]^-}$	-36.768	4.658 / 49.676	-91.102	-109.836	18.734	-55.502
$\mathbf{Br-I\cdots Br^-}$	-29.772	14.066 / 31.566	-75.405	-75.992	0.588	-30.360
$\mathbf{[Br-I-Br]^-}$	-35.384	10.219 / 44.020	-89.623	-95.168	5.545	-40.929
$\mathbf{I-Cl\cdots I^-}$	-16.528	3.934 / 26.530	-46.993	-61.051	14.058	-30.587
$\mathbf{[I-Cl-I]^-}$	-21.562	-0.093 / 61.931	-83.401	-101.596	18.195	-39.758
$\mathbf{I-Br\cdots I^-}$	-23.592	4.283 / 32.005	-59.880	-73.617	13.737	-37.329
$\mathbf{[I-Br-I]^-}$	-26.751	-2.072 / 54.507	-79.187	-99.505	20.318	-47.069
$\mathbf{I-I\cdots I^-}$	-27.159	7.186 / 32.084	-66.430	-75.452	9.022	-36.181
$\mathbf{[I-I-I]^-}$	-29.709	1.892 / 45.732	-77.333	-93.320	15.988	-45.696

that our IQA deformations do not include properly relativistic effects, although this does not affect the E_{int} values reported.

The E_{def} values of the attacking anions are considerably bigger than those of the diatomic fragment. This can be explained by the larger number of relaxation channels (or degrees of freedom) of the latter. Interestingly, the E_{def}'s of $[I-Cl-I]^-$ and $[I-Br-I]^-$ systems are negative, a fact related with the energy stabilisation of any fragment that gains electrons. After all, halogens have high electron affinities. Notice how the deformation of the X_1-Y_2 group decreases as we go down the table. Iodine containing systems display very small E_{def}'s. As the halide

approaches to the halogen diatomic, two energetically opposed factors balance the deformation in the $X_1 - Y_2$ system: an increasing electronic cost and an also increasing electron affinity-driven charge transfer stabilisation. This two factors operate in unison in the halide deformation, since it gets depopulated as well as electronically deformed.
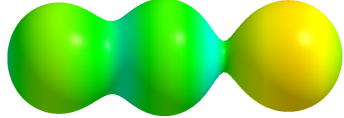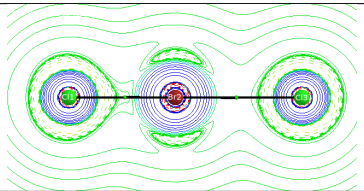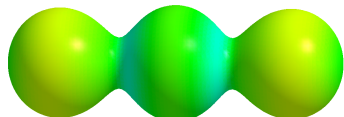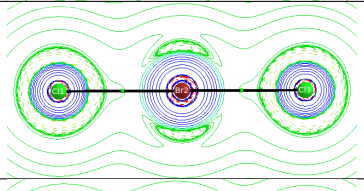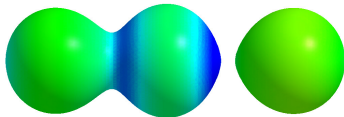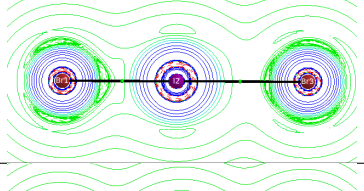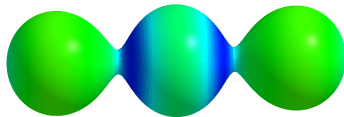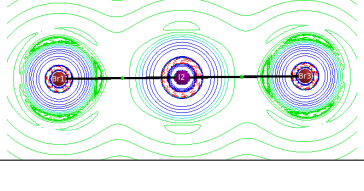
Turning to the electrostatic part of the interaction between the two fragments, E_{class} is seen to correlate with E_{form}. Indeed, the asymmetric complexes $X_1 - Y_2 \cdots X_3{}^-$, that experience smaller deformations and lower classical interaction energies, present slightly destabilising or even stabilising E_{class} values depending on the polarisant-polarisable character of the central and σ-hole featuring atom and the attacking halide. Such behaviour is generally consistent with lower formation energies, and points out the relevance of electrostatics in describing these XB systems. In fact, as pointed out by Clark et al.,[88,89] the ESP calculated at specific points is shown to correlate well with E_{form}. Nevertheless, as can be appreciated from Table 3, the complex formation cannot be explained in terms of electrostatics only; by contrast, it is the non-classical E_{xc} the component that accounts for most of the total E_{int} as it is in all cases negative and represents a stronger interaction between fragments $X_1 - Y_2$ and $X_3{}^-$.

These findings contrast with those obtained with EDA by Wolters and Bickelhaupt,[48] who reported stabilising electrostatic energies for all the trihalides here considered. This is what is normally expected from the use of interpenetrating electron densities. In EDA or SAPT, when the density of a fragment spreads over a region close to the nuclei of the other fragment, a large stabilising contribution appears which is absent in exhaustive spatial partitionings. In our opinion, large EDA electrostatic stabilisations simply signal the inadequacy of the interpenetrating model, for an electron close to the nucleus of another fragment should be associated to the latter and not to the former. Otherwise, the trends in the evolution of the different EDA contributions run roughly parallel to our IQA results.

The last energy descriptor reported here accounts for the Pauli repulsion at long range regime.[90] The fact that XCR is negative in all the cases explored is a very strong indicator of the non-perturbative regime of these interactions and of the fundamental role played by orbital interactions, in standard molecular orbital parlance, or covalency or exchange-correlation effects in real space language. Negative XCRs imply that exchange-correlation overcomes deformation, signalling the importance of electron delocalisation overcoming Pauli repulsion. We observe, once and again, that these simple XB models cannot be understood fully in terms of electrostatics.

4.5. Other topological descriptors: The Laplacian of ρ and the electrostatic potential

Table 4: Electrostatic potential on the 0.05 a.u. isosurface of ρ (left) and Laplacian of the electron density on a molecular plane (right) for $Cl-Br\cdots Cl$, $[Cl-Br-Cl]^-$, $[Br-I\cdots Br-]$ and $[Br-I-Br]^-$. A red to blue palette has been used ranging from -0.22 to +0.22 a.u. for the ESP and from 1.00 to +1.00 a.u. in the case of the Laplacian.

System	ESP on $\rho = 0.05$	$\nabla^2\rho$ on a plane
$\mathbf{Cl-Br\cdots Cl^-}$		
$\mathbf{[Cl-Br-Cl]^-}$		
$\mathbf{Br-I\cdots Br^-}$		
$\mathbf{[Br-I-Br]^-}$		

In order to complete the above quantitative energetic analysis, we now turn to the usual qualitative insights that can be obtained from inspecting both the electrostatic potential (ESP) and the Laplacian of the electron density, $\nabla^2\rho(\boldsymbol{r})$. The complete set of representations can be found inn the SI (Tables S5-S9). Here, we show two representative $X_1-Y_2-X_3{}^-$ systems: $Cl-Br-Cl^-$ and $Br-I-Br^-$. Table 4 presents the ESP mapped onto a $\rho(\boldsymbol{r}) = 0.05$ a.u. isosurface, along with 2D Laplacian maps using solid lines for positive values and dashed lines for negative ones.

σ-holes are clearly present as blueish ESP regions along the bonding direction. A very clear evolution from the more polarising Cl atom to the more polarisable I moiety is clearly seen. The Laplacian counts the correct number of shells only for chlorine, but can be clearly used to unveil the σ-holes in all cases: unprotected, depletion regions, together with torus-like lone pair accumulation regions, are notorious along the molecular axis in the central atoms. Tables

S5-S9 show that the iodine lone pairs can even be discerned as the red, less positive regions of $\nabla^2\rho$ when of the anions and the diatomic species are depicted, disclose the characteristic clear directionality in the σ-holes. For instance, in the case of the compact chlorine atoms, a flattening of the external negative Laplacian regions is visible when close to another polarising entity. Conversely, when chlorine occupies the external positions (i.e., X=Cl) the outermost concentration distorts towards the central atom (e.g., $Cl-Br\cdots Cl^-$).

We will not proceed further. Using the ESP and $\nabla^2\rho(\boldsymbol{r})$ (or the ELF) has become mainstream and needs no more consideration. Both can be used to sense and detect σ-holes. However we should not forget that the information they provide is qualitative in nature. For example, (i) the most positive ESP is found for I atoms, independently of whether they occupy the central position or not, and (ii) the Laplacian detects different shells for different atoms, so that quantification becomes very difficult with it. Moreover, we insist that standard ESP representations do not account for the whole charge distribution and that their bare use might be misleading. As an example, the most intense σ-holes as sensed from the ESP are actually those of iodine that give rise to the lowest interatomic E_{class} values (see Table 1). However, when I occupies the edge position (Table S7) and thus it becomes the attacking halide for complexes $X_1-Y_2\cdots X_3$, its electrostatic energies with central and more electronegative Cl and Br atoms are highly destabilising. This is another example of the incomplete picture that the ESP provides.

5. Conclusions

We examine in this work a minimal model of halogen bond (XB) interactions in an attempt to understand their nature beyond the σ-holes electrostatic picture under an orbital-invariant perspective. To that end, we have investigated a set of negatively charged halogen triatomic species built with different combinations of Cl, Br and I. Given the controversial character of halogen bonding with F containing species, fluorine has not been considered. For all possible Cl, Br, I combinations, two linear geometries have been selected: the trihalide optimised one together with another that mimics an XB. The latter is obtained by constraining the interatomic distance of two of the atoms at their experimental gas-phase value while a halide anion attacks the constrained diatomic. We have used the interacting quantum atoms (IQA) approach to dissect the energetics of the systems, complementing it with other traditional descriptors like electrostatic potential (ESP) or electron density Laplacian maps.

Both the ESP and the Laplacian analyses reveal the traditional signature of σ-holes: positive regions of the ESP when mapped onto an isodensity or van der Waals surface, and charge depletion areas of the Laplacian field. A neat distinction between different atoms also emerges. Chlorine preserves its atomic shell structure to a large extent, while bromine and iodine are largely deformed according to their more polarisable nature. Similarly, the more polarisant-polarisable difference in the atomic pair that interacts, the clearer the σ-hole develops.

The QTAIM's charges assigned to each atom within the anionic species unveil a profound density polarisation and concomitant charge transfer, that in light of a Y_2-X_3 distance scan takes place gradually with participation of just the charge donor and its farthermost partner, while the central atom remains a spectator. These findings support the assumption that these systems present 3c-4e bonds, which spread the anionic charge over the X_1X_2 terminal atoms, that present anomalously large delocalisation indexes.

The electrostatic σ-hole model is shown to be useful as a qualitative tool but far from the real energetics of the complexes. Indeed, the presence of such a positive region in the ESP does not necessarily imply global favourable electrostatics between the interacting species, that account for the whole charge distribution, and such a simple interpretation may become misleading. Thus, we have shown that in all but those cases where the XB involves a very polarisant-polarisable interacting pair the full electrostatic interaction between the halide and the remaining diatomic is destabilising. This contrasts other energy decomposition analyses

characterised by interpenetrating densities, which tend to provide stabilising electrostatic contributions due to the non-physical overlap of the densities of the two fragments.

Taking into account the non-negligible deformation energies suffered by both entities, it is the covalent (exchange-correlation) interaction that justifies the overall stability of the complexes. This is in line with what prior studies had suggested in other systems of interest. By reducing the complexity of the systems here studied to an absolute minimum, we believe to have shown convincingly that electrostatics alone is not enough to understand the stability of halogen bonded systems. Together with the evolution of charge transfer, the essential role of electron delocalisation, i.e., of orbital interactions, is thus highlighted.

6. Acknowledgements

7. Data availability statement

The data that support the findings of the present study are available in both the article and its supplementary material. Additional information can be requested from the authors.

8. ORCID

Fernando Jiménez-Grávalos https://orcid.org/0000-0002-9181-5234

Miguel Gallegos https://orcid.org/0000-0001-7472-8158

Ángel Martín Pendás https://orcid.org/0000-0002-4471-4000

Alexander S. Novikov https://orcid.org/0000-0001-9913-5324

References

[1] B. S. Sumerlin, *Science* **2018**, *362*, 150–151.

[2] P. Hobza, J. Řezáč, *Chemical Reviews* **2016**, *116*, 4911–4912.

[3] C. F. J. Faul, *Accounts of Chemical Research* **2014**, *47*, 3428–3438.

[4] D. Y. Lee, Z. Khatun, J.-H. Lee, Y. kyu Lee, I. In, *Biomacromolecules* **2011**, *12*, 336–341.

[5] J. J. Strunk, I. Gregor, Y. Becker, P. Lamken, S. Lata, A. Reichel, J. Enderlein, J. Piehler, *Bioconjugate Chemistry* **2009**, *20*, 41–46.

[6] J. Hermann, R. A. DiStasio, A. Tkatchenko, *Chemical Reviews* **2017**, *117*, 4714–4758.

[7] B. Rybtchinski, *ACS Nano* **2011**, *5*, 6791–6818.

[8] W. Zhan, T. Wei, Q. Yu, H. Chen, *ACS Applied Materials & Interfaces* **2018**, *10*, 36585–36601.

[9] C. Sutton, C. Risko, J.-L. Brédas, *Chemistry of Materials* **2015**, *28*, 3–16.

[10] J. S. Pallesen, K. T. Tran, A. Bach, *Journal of Medicinal Chemistry* **2018**, *61*, 8088–8103.

[11] A. Minecka, E. Kaminska, M. Tarnacka, I. Grudzka-Flak, M. Bartoszek, K. Wolnica, M. Dulski, K. Kaminski, M. Paluch, *Molecular Pharmaceutics* **2018**, *15*, 4764–4776.

[12] J.-P. Correa-Baena, M. Saliba, T. Buonassisi, M. Grätzel, A. Abate, W. Tress, A. Hagfeldt, *Science* **2017**, *358*, 739–744.

[13] A. J. Neel, M. J. Hilton, M. S. Sigman, F. D. Toste, *Nature* **2017**, *543*, 637–646.

[14] F. D. Toste, M. S. Sigman, S. J. Miller, *Accounts of Chemical Research* **2017**, *50*, 609–615.

[15] S. E. Wheeler, T. J. Seguin, Y. Guan, A. C. Doney, *Accounts of Chemical Research* **2016**, *49*, 1061–1069.

[16] S. A. Kholodar, A. K. Ghosh, K. Świderek, V. Moliner, A. Kohen, *Proceedings of the National Academy of Sciences* **2018**, *115*, 10311–10314.

[17] M. Yáñez, P. Sanz, O. Mó, I. Alkorta, J. Elguero, *Journal of Chemical Theory and Computation* **2009**, *5*, 2763–2771.

[18] J. S. Murray, P. Lane, P. Politzer, *Journal of Molecular Modeling* **2008**, *15*, 723–729.

[19] J. S. Murray, P. Lane, P. Politzer, *International Journal of Quantum Chemistry* **2007**, *107*, 2286–2292.

[20] J. S. Murray, P. Lane, T. Clark, P. Politzer, *Journal of Molecular Modeling* **2007**, *13*, 1033–1038.

[21] J. Y. Lim, P. D. Beer, *Chem* **2018**, *4*, 731–783.

[22] M. H. Kolář, P. Hobza, *Chemical Reviews* **2016**, *116*, 5155–5187.

[23] H. Wang, W. Wang, W. J. Jin, *Chemical Reviews* **2016**, *116*, 5072–5104.

[24] L. C. Gilday, S. W. Robinson, T. A. Barendt, M. J. Langton, B. R. Mullaney, P. D. Beer, *Chemical Reviews* **2015**, *115*, 7118–7195.

[25] G. Cavallo, P. Metrangolo, R. Milani, T. Pilati, A. Priimagi, G. Resnati, G. Terraneo, *Chemical Reviews* **2016**, *116*, 2478–2601.

[26] P. Politzer, J. S. Murray, T. Clark, *Physical Chemistry Chemical Physics* **2013**, *15*, 11178.

[27] P. Politzer, J. S. Murray, *ChemPhysChem* **2020**, *21*, 579–588.

[28] L. P. Wolters, P. Schyman, M. J. Pavan, W. L. Jorgensen, F. M. Bickelhaupt, S. Kozuch, *Wiley Interdisciplinary Reviews: Computational Molecular Science* **2014**, *4*, 523–540.

[29] P. J. Costa, *Physical Sciences Reviews* **2017**, *2*.

[30] L. P. Wolters, N. W. G. Smits, C. F. Guerra, *Physical Chemistry Chemical Physics* **2015**, *17*, 1585–1592.

[31] M. Novák, C. Foroutan-Nejad, R. Marek, *Physical Chemistry Chemical Physics* **2015**, *17*, 6440–6450.

[32] P. L. Bora, M. Novák, J. Novotný, C. Foroutan-Nejad, R. Marek, *Chemistry - A European Journal* **2017**, *23*, 7315–7323.

[33] J. Thirman, E. Engelage, S. M. Huber, M. Head-Gordon, *Physical Chemistry Chemical Physics* **2018**, *20*, 905–915.

[34] M. A. Blanco, Á. Martín Pendás, E. Francisco, *Journal of Chemical Theory and Computation* **2005**, *1*, 1096–1109.

[35] E. Francisco, Á. Martín Pendás, M. Á. Blanco, *Journal of Chemical Theory and Computation* **2005**, *2*, 90–102.

[36] O. A. Syzgantseva, V. Tognetti, L. Joubert, *The Journal of Physical Chemistry A* **2013**, *117*, 8969–8980.

[37] M. Yahia-Ouahmed, V. Tognetti, L. Joubert, *Computational and Theoretical Chemistry* **2015**, *1053*, 254–262.

[38] M. Yahia-Ouahmed, V. Tognetti, L. Joubert, *Theoretical Chemistry Accounts* **2016**, *135*.

[39] K. Eskandari, M. Lesani, *Chemistry - A European Journal* **2015**, *21*, 4739–4746.

[40] H. J. Jahromi, K. Eskandari, A. Alizadeh, *Journal of Molecular Modeling* **2015**, *21*.

[41] G. Buralli, A. Petelski, N. Peruchena, G. Sosa, D. Duarte, *Molecules* **2017**, *22*, 2034.

[42] J. M. Guevara-Vela, D. Ochoa-Resendiz, A. Costales, R. Hernández-Lamoneda, Á. Martín Pendás, *ChemPhysChem* **2018**, *19*, 2512–2517.

[43] N. Orangi, K. Eskandari, J. C. R. Thacker, P. L. A. Popelier, *ChemPhysChem* **2019**, *20*, 1922–1930.

[44] I. Alkorta, A. F. Silva, P. L. A. Popelier, *Molecules* **2020**, *25*, 2674.

[45] T. Sakurai, M. Sundaralingam, G. A. Jeffrey, *Acta Crystallographica* **1963**, *16*, 354–363.

[46] G. R. Desiraju, R. Parthasarathy, *Journal of the American Chemical Society* **1989**, *111*, 8725–8726.

[47] T. Bui, S. Dahaoui, C. Lecomte, G. Desiraju, E. Espinosa, *Angewandte Chemie International Edition* **2009**, *48*, 3838–3841.

[48] L. P. Wolters, F. M. Bickelhaupt, *ChemistryOpen* **2012**, *1*, 96–105.

[49] C. Foroutan-Nejad, Z. Badri, R. Marek, *Physical Chemistry Chemical Physics* **2015**, *17*, 30670–30679.

[50] C. Foroutan-Nejad, *Angewandte Chemie International Edition* **2020**, *59*, 20900–20903.

[51] P. L. A. Popelier in *Intermolecular Forces and Clusters I*, Springer Berlin Heidelberg, **2005**, pp. 1–56.

[52] R. F. W. Bader, *Atoms in Molecules: A Quantum Theory (International Series of Monographs on Chemistry)*, Clarendon Press, **1994**.

[53] X. Fradera, M. A. Austen, R. F. W. Bader, *The Journal of Physical Chemistry A* **1999**, *103*, 304–314.

[54] E. Francisco, J. L. Casals-Sainz, T. Rocha-Rinza, Á. Martín Pendás, *Theoretical Chemistry Accounts* **2016**, *135*.

[55] T. Clark, M. Hennemann, J. S. Murray, P. Politzer, *Journal of Molecular Modeling* **2007**, *13*, 291–296.

[56] T. Clark, *Wiley Interdisciplinary Reviews: Computational Molecular Science* **2012**, *3*, 13–20.

[57] A. D. Becke, K. E. Edgecombe, *The Journal of Chemical Physics* **1990**, *92*, 5397–5403.

[58] K. Eskandari, H. Zariny, *Chemical Physics Letters* **2010**, *492*, 9–13.

[59] D. J. R. Duarte, G. L. Sosa, N. M. Peruchena, *Journal of Molecular Modeling* **2012**, *19*, 2035–2041.

[60] V. Tognetti, L. Joubert, *Theoretical Chemistry Accounts* **2015**, *134*.

[61] M. J. Frisch, G. W. Trucks, H. B. Schlegel, G. E. Scuseria, M. A. Robb, J. R. Cheeseman, G. Scalmani, V. Barone, B. Mennucci, G. A. Petersson, H. Nakatsuji, M. Caricato, X. Li, H. P. Hratchian, A. F. Izmaylov, J. Bloino, G. Zheng, J. L. Sonnenberg, M. Hada, M. Ehara, K. Toyota, R. Fukuda, J. Hasegawa, M. Ishida, T. Nakajima, Y. Honda, O. Kitao, H. Nakai, T. Vreven, J. A. Montgomery, Jr., J. E. Peralta, F. Ogliaro, M. Bearpark, J. J. Heyd, E. Brothers, K. N. Kudin, V. N. Staroverov, T. Keith, R. Kobayashi, J. Normand, K. Raghavachari, A. Rendell, J. C. Burant, S. S. Iyengar, J. Tomasi, M. Cossi, N. Rega, J. M. Millam, M. Klene, J. E. Knox, J. B. Cross, V. Bakken, C. Adamo, J. Jaramillo, R. Gomperts, R. E. Stratmann, O. Yazyev, A. J. Austin, R. Cammi, C. Pomelli, J. W. Ochterski, R. L. Martin, K. Morokuma, V. G. Zakrzewski, G. A. Voth, P. Salvador, J. J. Dannenberg, S. Dapprich, A. D. Daniels, O. Farkas, J. B. Foresman, J. V. Ortiz, J. Cioslowski, , D. J. Fox, *Gaussian09 Revision D.01*, Gaussian Inc., Wallingford CT, 2013.

[62] S. Grimme, J. Antony, S. Ehrlich, H. Krieg, *The Journal of Chemical Physics* **2010**, *132*, 154104.

[63] Y. Zhao, D. G. Truhlar, *Theoretical Chemistry Accounts* **2007**, *120*, 215–241.

[64] A. Bauzá, I. Alkorta, A. Frontera, J. Elguero, *Journal of Chemical Theory and Computation* **2013**, *9*, 5201–5210.

[65] N. Mardirossian, M. Head-Gordon, *Journal of Chemical Theory and Computation* **2016**, *12*, 4303–4325.

[66] Y. Wang, P. Verma, X. Jin, D. G. Truhlar, X. He, *Proceedings of the National Academy of Sciences* **2018**, *115*, 10257–10262.

[67] A. S. Mikherdov, A. S. Novikov, V. P. Boyarskiy, V. Y. Kukushkin, *Nature Communications* **2020**, *11*, 2921.

[68] A. S. Ostras', D. M. Ivanov, A. S. Novikov, P. M. Tolstoy, *Molecules* **2020**, *25*, 1406.

[69] M. A. Kryukova, D. M. Ivanov, M. A. Kinzhalov, A. S. Novikov, A. S. Smirnov, N. A. Bokach, V. Y. Kukushkin, *Chemistry – A European Journal* **2019**, *25*, 13671–13675.

[70] M. V. Kashina, M. A. Kinzhalov, A. S. Smirnov, D. M. Ivanov, A. S. Novikov, V. Y. Kukushkin, *Chemistry – An Asian Journal* **2019**, *14*, 3915–3920.

[71] M. A. Kinzhalov, M. V. Kashina, A. S. Mikherdov, E. A. Mozheeva, A. S. Novikov, A. S. Smirnov, D. M. Ivanov, M. A. Kryukova, A. Y. Ivanov, S. N. Smirnov, V. Y. Kukushkin, K. V. Luzyanin, *Angewandte Chemie International Edition* **2018**, *57*, 12785–12789.

[72] W. Liu, D. Peng, *The Journal of Chemical Physics* **2009**, *131*, 031104.

[73] D. M. Ivanov, S. V. Baykov, A. S. Novikov, G. Romanenko, N. A. Bokach, R. A. Evarestov, V. Y. Kukushkin, *Crystal Growth & Design* **2020**, *20*, 3417–3428.

[74] D. S. Bolotin, M. V. Il'in, V. V. Suslonov, A. S. Novikov, *Symmetry* **2020**, *12*, 637.

[75] A. S. Mikherdov, S. A. Katkova, A. S. Novikov, M. M. Efremova, E. Y. Reutskaya, M. A. Kinzhalov, *CrystEngComm* **2020**, *22*, 1154–1159.

[76] D. S. Bolotin, N. S. Soldatova, M. Y. Demakova, A. S. Novikov, D. M. Ivanov, I. S. Aliyarova, A. Sapegin, M. Krasavin, *Inorganica Chimica Acta* **2020**, *504*, 119453.

[77] T. Nakajima, K. Hirao, *Chemical Physics Letters* **1999**, *302*, 383–391.

[78] F. Lovas, *Diatomic Spectral Database, NIST Standard Reference Database 114*, **2002**. http://www.nist.gov/pml/data/msd-di/index.cfm.

[79] Q. Sun, T. C. Berkelbach, N. S. Blunt, G. H. Booth, S. Guo, Z. Li, J. Liu, J. D. McClain, E. R. Sayfutyarova, S. Sharma, S. Wouters, G. K.-L. Chan, *Wiley Interdisciplinary Reviews: Computational Molecular Science* **2018**, *8*, e1340.

[80] Á. Martín Pendás, E. Francisco, *Promolden. A QTAIM/IQA code (unpublished)*.

[81] *AIMAll (Version 17.11.14), Todd A. Keith, TK Gristmill Software, Overland Park KS, USA, 2017 (aim.tkgristmill.com).*

[82] *Jmol: an open-source Java viewer for chemical structures in 3D. http://www.jmol.org/.*

[83] J. D. Hunter, *Computing in Science & Engineering* **2007**, *9*, 90–95.

[84] G. C. Pimentel, *The Journal of Chemical Physics* **1951**, *19*, 446–448.

[85] R. E. Rundle, *The Journal of Physical Chemistry* **1957**, *61*, 45–50.

[86] Á. Martín Pendás, E. Francisco, *ChemPhysChem* **2019**, *20*, 2722–2741.

[87] V. Oliveira, E. Kraka, D. Cremer, *Physical Chemistry Chemical Physics* **2016**, *18*, 33031–33046.

[88] T. Clark, J. S. Murray, P. Politzer, *ChemPhysChem* **2018**, *19*, 3044–3049.

[89] J. S. Murray, P. Politzer, *Crystals* **2020**, *10*, 76.

[90] E. Francisco, A. Martín Pendás in *Non-Covalent Interactions in Quantum Chemistry and Physics*, A. Otero de la Roza, G. A. DiLabio (Eds.), Elsevier, **2017**, pp. 27 – 64.